SEMARAK ILMU PUBLISHING

Journal of Advanced Research in Fluid Mechanics and Thermal Sciences

Journal homepage:
https://semarakilmu.com.my/journals/index.php/fluid_mechanics_thermal_sciences/index
ISSN: 2289-7879

Influence of Altered Pressures on Flow Dynamics in Carotid Bifurcation System Using Numerical Methods

Abhilash Hebbandi Ningappa[1], Suraj Patil[1], Gowrava Shenoy Belur[1], Augustine Benjamin Valerian Barboza[1], Nitesh Kumar[1], Raghuvir Pai Ballambat[1], Adi Azriff Basri[2], Shah Mohammed Abdul Khader[1,*], Masaaki Tamagawa[3]

[1] Department of Mechanical Engineering and Industrial Engineering, Manipal Institute of Technology, Manipal Academy of Higher Education, Manipal, 576104, Karnataka, India
[2] Department of Aerospace Engineering, Universiti Putra Malaysia, Selangor, Malaysia
[3] Department of Biological Functions Engineering, Graduate School of Life Sciences and System Engineering, Kyushu Institute of Technology, Japan

ARTICLE INFO

Article history:
Received 18 March 2022
Received in revised form 22 May 2022
Accepted 31 May 2022
Available online 27 June 2022

Keywords:
Carotid bifurcation; ANSYS Fluent; altered blood pressure; CFD; blood flow

ABSTRACT

The application of numerical methods like CFD to understand hemodynamics in arteries has excellent potential to solve complex flow problems. In recent years, CFD has been primarily used in the hemodynamics of the carotid artery due to advances in computational resources. This technique is widely used to obtain knowledge on hemodynamics, predict the risk factors for the development and progression of the atherosclerotic lesion, and analyze local flow profiles due to changes in the carotid artery geometry. This fundamental study will be supportive in observing the blood flow behavior through arteries and studying arterial diseases. The present study investigates three different subject-specific carotid bifurcation models under altered blood pressure conditions. Subject-specific 3D carotid bifurcation modeling is carried out using Materialize software. Unsteady flow simulation is conducted in ANSYS Fluent under the rigid wall and Newtonian conditions. The haemodynamic parameters such as vorticity, helicity, and time-averaged wall shear stress (TAWSS) were evaluated to understand better the beginning and progression of atherosclerotic plaques in the bifurcation. Also, the influence of geometric variation in the bifurcation region was investigated, and it was observed that this region causes significant vortex formation zones. A noticeable reduction in velocity and backflow formation was observed, which reduced the shear stress. It is established that the regions of low TAWSS along the bifurcation region are likely to develop atherosclerosis.

1. Introduction

The recent advances in the computation domain have simplified the exploration of emerging multidisciplinary areas. At present computational simulations in the biomedical area support clinicians in decision making. Applications of simulations available in a broad spectrum aid the prognosis and complimenting the diagnostic modalities so far [1,2]. Computational fluid dynamics

* *Corresponding author.*
E-mail address: smak.quadri@manipal.edu

https://doi.org/10.37934/arfmts.97.1.4761

(CFD) and Fluid-Structure interaction (FSI) simulations of blood flow in flexible arteries provide the quantitative visualization of flow in the cardiovascular system, thereby aiding the researchers and clinicians in gaining a better understanding of the cardiovascular pathology [3]. In the near future, radiological data collected from patients post computational simulation processing shall help the doctors in treatment decision-making [4]. CFD emerged as a popular non-invasive methodology to access the hemodynamics, providing assessment details on blood pressure, velocity, shear stress, etc., through which disease initiation and progression can be hypothesized [5]. Many studies have been conducted using the CFD and FSI technique to determine the vascular disease's blood flow behavior. Physiologically realistic CFD simulations of pulsatile blood flow in normal and occluded arteries help estimate the forces acting on the elastic wall to predict rupture-prone regions in the artery. This has value addition in diagnosing and treating stenosis and related diseases. The flow was observed to strongly relate to velocity waves, especially post stenosis region. In addition, recirculation and reverse flow regions were found post stenosis [6-9].

The carotid artery is the prominent artery located on the left and right side of the neck that supplies blood to the face, brain, and neck portions. Oxygenated blood from the aorta flows into Common Carotid Artery (CCA) and other branches into Internal Carotid Artery (ICA) and External Carotid Artery (ECA). At the branching of these two divisions, a widening of CCA is called a carotid bulb or sinus. The carotid sinus is the region of interest because the common carotid extends and branches into the internal and external carotid [10]. The blood flow pattern in the sinus region is disturbed, leading to plaque accumulation. The disturbed shear created in carotid bifurcation is due to the Helical flow of blood [11,12]. Inside the artery, soft structures accumulate in the form of irregular and arbitrary shapes, leading to plaque deposition and hardening. In this irregular area, platelets fill cracks, creating blood clots in arteries, resulting in atherosclerosis. Zones where artery bifurcates and zones of arterial inner curvature are susceptible to plaque build-up [13-16]. Plaques are limitedly localized to the zones of low wall shear stress (WSS). At the high WSS region, the chances of formation of atherosclerosis are less. The study of blood flow in the normal carotid artery can be useful in studying the influence of Haemodynamics on the formation of plaque [17,18]. From the analysis, various output parameters related to the flow of blood can be determined and evaluation can be done based on the value of WSS observed in the particular region. Some of the researchers have considered the stenosed geometry for the simulation and disturbance in the flow due to the presence of stenosis is determined [19,20]. Severe stenosis in the carotid artery indicates the possibility of stroke risk. However, the stroke chances also depend on major factors like arterial geometry, age etc. Hence, there are reported cases of severe carotid artery stenosis that haven't suffered a stroke, while cases with mild to moderate stenosis reportedly have suffered a stroke [21-23]. Transport and flow-induced activation of platelets due to the influence of disturbed flow is caused by the presence of stenosis. To get an accurate solution the chosen boundary condition should be similar to the patient-specific [24]. The velocity and flowrate profile can be obtained by two methods Doppler ultrasound [17,20] and Phase-contrast MRI [8,12]. In many of the studies flow of blood is considered Newtonian, neglecting the shear-thinning effect, in the regions like stenosis blood flow will be non-Newtonian [20,21,24,25]. Moyle *et al.,* studied the variation of the flow in the carotid artery due to different inlet conditions. The study was focused on investigating the sensitivity of parameters like WSS and FSI for change in secondary flow [26]. Generation of secondary flow profile was done using sufficient long entrance length, to which helical pitch and curvature were added. It was observed that the influence of geometric variation on the WSS and Oscillatory Shearing Index is comparatively more than the influence due to vessel curvature-related velocity profile at the inlet [27]. Campbell *et al.,* studied the influence of inlet velocity profile for analyzing flow in patient-specific carotid bifurcation. The effect of different idealized inlet velocity profiles like blunt, parabolic,

and Womersley flow concerning patient-specific velocity profiles was studied [28]. Pointwise percentage error of mean WSS and OSI were calculated, and similar values were calculated for the parabolic inlet velocity profile. So, it is suitable to use parabolic inlet velocity boundary conditions for the accurate CFD analysis.

Morbiducci *et al.,* studied the implications for indicators of abnormal flow at carotid bifurcation for outflow boundary conditions. Governing of blood flow depends on prescribing proper boundary conditions, investigation of outflow boundary condition assumptions is done using an image-based CFD model of the carotid artery [29]. Vascular wall dysfunction is identified with three key hemodynamic wall parameters. Nithiarasu *et al.,* studied the influences of domain extension at carotid bifurcation for a moderately stenosed patient-specific geometry. CFD simulation performed on patient-specific artery models with moderately severe stenosis investigates the influence of extensions in the domain outlets. WSS, OSI, and WSSAD were calculated. WSS was high near the apex of the carotid artery and near stenosis. The results obtained for outlet domain extension was having marginal influence [30]. The literature review finds that the majority of the analysis considers normal blood pressure. However, there aren't substantial flow dynamics studies that consider the effect of high and low blood pressure which is clinically very significant, since the adverse flow pressure has been proven fatal [6,7,8,31]. The present study considers anatomically different three carotid artery geometries for the investigation of hemodynamics at various blood pressures to prognosis for critical factors. A low-pressure condition can be a result of abnormal pumping action, widened artery, age, and several other factors, in which the flow pressure in arteries is less than the required for normal functioning of organs. Likewise, the effect of hypertension is also analyzed in various geometric variations in bifurcation to estimate the wall shear stress and derived parameters.

2. Methods

2.1 Theory of CFD

Blood flow in this vascular model is assumed to be Newtonian, laminar and incompressible [5, 8, 12]. The flow is assumed to be laminar as the blood flow is simulated under resting conditions of the cardiac cycle [32]. The governing equation used is the Navier-Stokes equation given by Eq. (1) and Eq. (2) [33].

$$\nabla . \upsilon \; = \; 0 \tag{1}$$

$$\rho \left(\frac{d\upsilon}{dt} \; + \; \upsilon . \nabla \upsilon \right) \; = \; -\nabla p \; + \; \mu \nabla^2 \upsilon \tag{2}$$

where ρ is the density, υ is the velocity vector, p is the pressure and μ is the dynamic viscosity of the fluid.

2.2 Modelling and Analysis

This study considers three different geometric shape subject-specific carotid bifurcation models for comparing the haemodynamic investigation as shown in Figure 1. A three-dimensional patient-specific model was created from CT-Angio data post-reconstruction using MIMICS 19 (Materialise, Leuven, Belgium) medical image processing software. Geometry construction steps are referred to from literature [33,34]. The carotid bifurcation models (1, 2 and 3) were discretized using polyhedral elements, as shown in Figure 2. The layered mesh closer to the boundary wall is also defined to

capture the effects of flow behavior as shown in the highlighted portion. Hybrid mesh is generated using Fluent meshing module wherein the mesh along the boundary wall contains octahedral elements and the interior is made up of hexahedral elements. The grid independence tests were carried out for all three models considering peak values for velocity inlet and pressure outlet. Change in velocity is monitored for change in grid size at CCA, ECA, and ICA. Figure 3 depicts the mesh independency test-taking velocity and pressure distribution respectively for model-1. A similar grid test is carried out on model-2 and 3. In the same locations, velocity is monitored for the other two cases. The grid test evaluation finds that velocity and pressure are normalized with the number of elements 350000 for model-1, 380000 for model-2, and 420000 for model-3. The analysis considers the constant dynamic viscosity of 0.004 N-s/m^2 and density of 1050 kg/m^3 for the fluid, as the flow in larger arteries with a high shear rate is Newtonian [12,19,33].

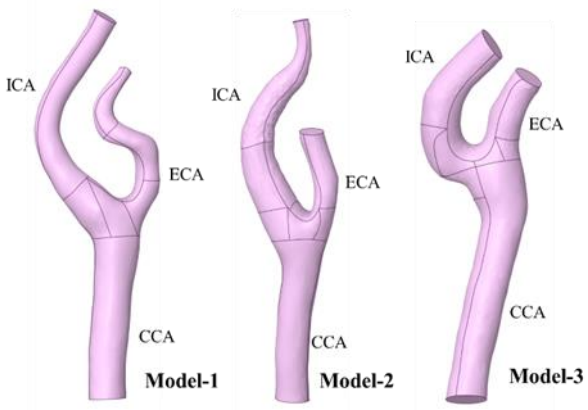

Fig. 1. Geometric details of 3D CAD models of carotid bifurcation

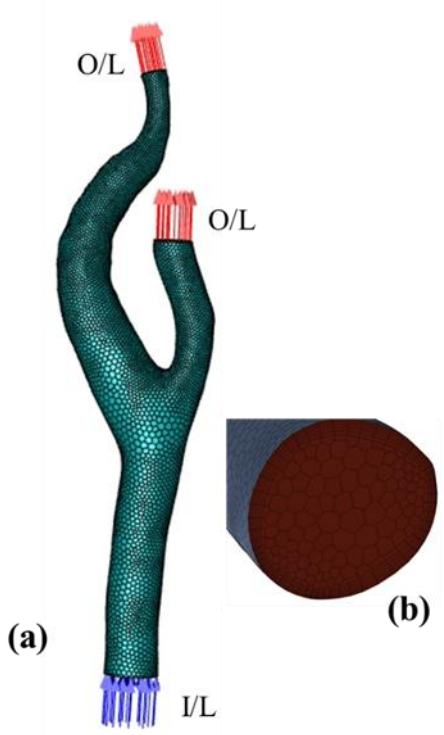

Fig. 2. Mesh description: (a) Polyhedra mesh in model-3 (b) Boundary wall mesh

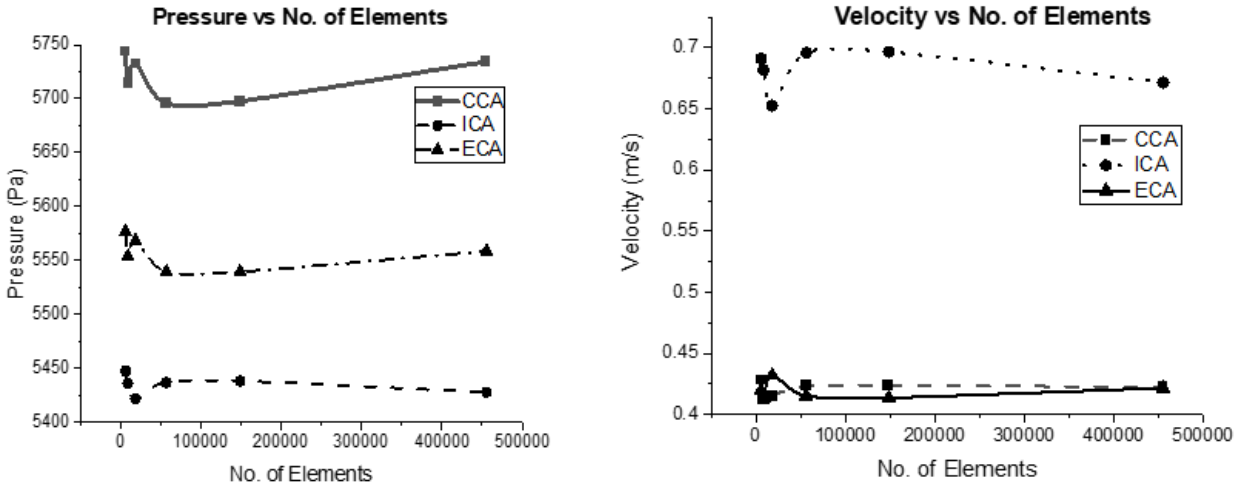

(a) (b)

Fig. 3. Grid dependency test details in model-1: (a) Pressure and (b) Velocity variation

Pulsatile velocity is defined at the inlet with a cardiac cycle of 0.8s as shown in Figure 4. Time-varying pressure waveform is defined at the outlet faces as shown in Figure 4. These time-varying pulsatile profiles were applied at the inlet and the outlet with the interpretation of a user-defined function, however, the walls of the models were assumed to be rigid [34,35,36]. Resistance type boundary condition is adopted at the outlet considering peripheral resistance under different pressure gradients such as normal blood pressure (NBP), High blood pressure (HBP), and Low blood pressure (LBP). The range of different blood pressure is normalized for comparison purposes to simulate physiological conditions variations of blood pressure. The methodology of inlet and outlet pulse wave generation is similar to that adopted in literature [4,37]. Pulsatile waveforms of velocity and pressure wave were divided into 180-time steps to capture flow behavior more precisely [33, 38]. The timestep independence conducted is depicted in figure 5 and each time step of 0.005 seconds for a total of 180-time steps is adopted to capture the flow behavior. Convergence criteria of $1x10^{-5}$ were employed to analyze the behavior of blood flow in these artery models [39,40].

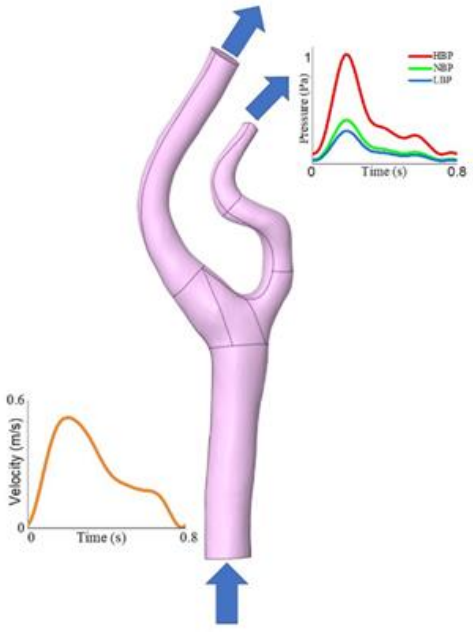

Fig. 4. Description of applied BC's (Time varying inlet velocity outlet pressure)

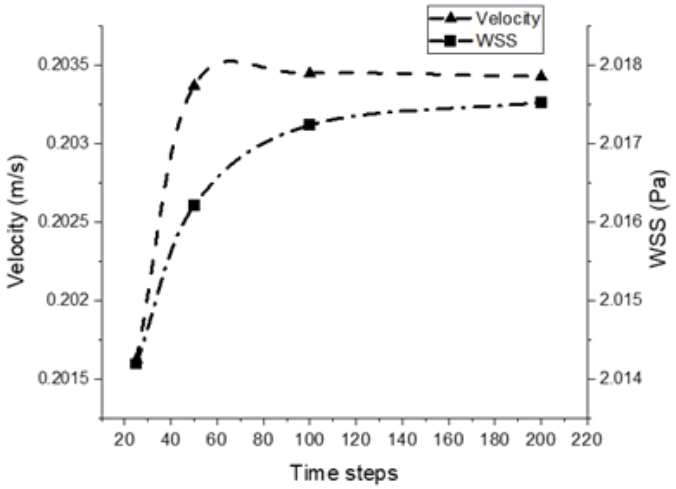

Fig. 5. Time dependency test details in model-2

3. Results

The results of the CFD analysis are compared for various input conditions. Three specific phases of the cardiac cycle; early systole (0.06s), peak systole (0.22s), and peak diastole (0.44s) were used to investigate haemodynamic factors like velocity, pressure, time-averaged wall shear stress, vorticity and helicity are that compared among three carotid artery models for various blood pressures. The simulations were carried out at different blood pressures demonstrating the importance of geometry variation at the bifurcation region. The flow rate of 70/30 distribution represents the upper physiological flow ratio between the ICA and ECA. The maximum changes in the flow occur during peak systole, hence this instant of pulse cycle is considered to describe and discuss the results obtained.

3.1 Velocity

Flow variation at the bifurcation region is being captured in different models in the form of velocity streamlines. Velocity contours plotted along with streamlines are shown in Figure 6 and 7 during peak systole and early diastole in three carotid bifurcation models at different blood pressures. The ECA of Model-2 and 3 are similar in geometric nature in contrast to model-1 which is highly tortuous which is evident from the velocity behavior profile. The CCA profile is straight in all three carotid models and has similar velocity behavior. In all three models, the flow is characterized by a steep velocity gradient at the bifurcation region and stagnant/reversed flow along the outer wall of the ICA. Because of the different geometric profiles of ICA branching in three models, the flow velocity is higher in ICA than in ECA in model-2 and 3, while in model-3, the flow is equally distributed with slightly higher magnitude in ICA than in ECA. Due to the higher curvature of ICA than ECA in bifurcation models, the flow separation occurs mainly in the outer wall of ICA with the increased flow towards the inner wall of ICA as clinically observed [12,42,43]. At peak systole along the center line of geometry, 50% magnitude of peak velocity value is observed in CCA of all three models. However, due to velocity gradients recirculation zones were observed in Model-3 near the outer wall of ECA. It is observed that in all three models towards the inner wall of ECA flow is aligned to the geometry of the artery. In ICA due to curvature Model-1 velocity streamlines are tortuous, whereas in the case of Model-2 & 3 having streamlines aligned to geometry during peak systole. During early diastole, CCA observed streamline flow until the bifurcation in Model-3, whereas Model-1 & 2 had recirculation near the inner wall and outer wall zones respectively due to steep velocity gradients. The case of ECA

in Model 1 has streamline flow whereas Model-2 and 3 have twisting streamlines along with the geometry during early diastole [32, 40, 43]. Flow in ICA of Model-1 is disturbed due to curvature, whereas Model-2 and Model-3 observed geometry aligned flow with maximum velocity near the inner wall.

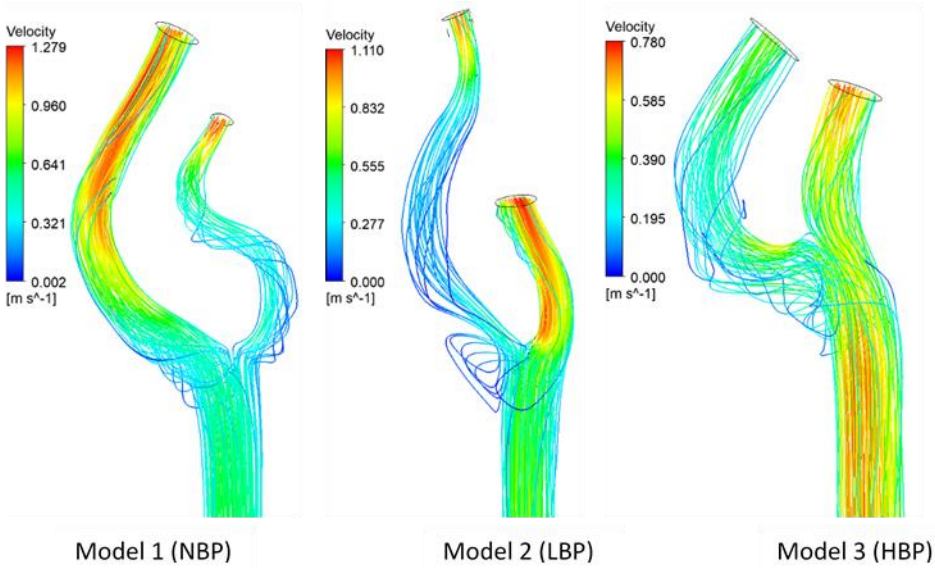

Fig. 6. Velocity streamlines in different carotid bifurcation models during peak systole at different outlet pressure

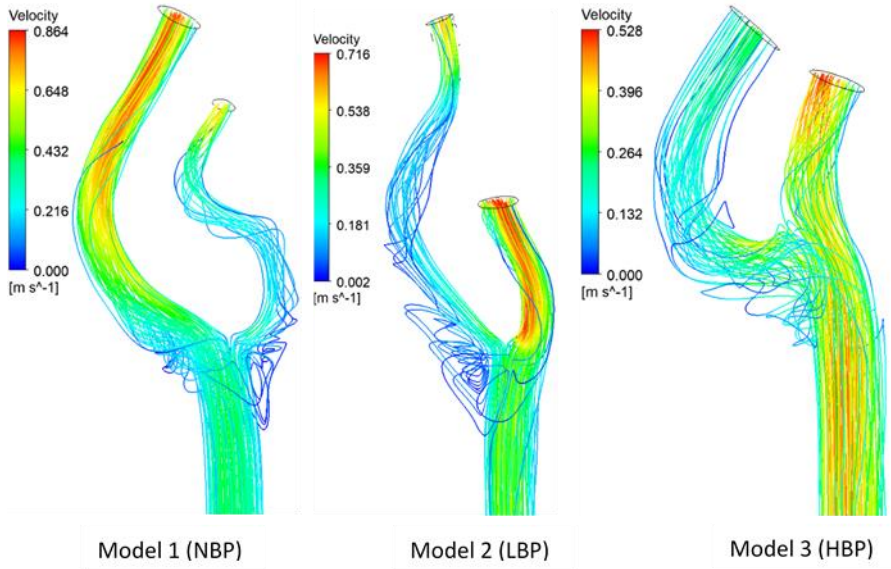

Fig. 7. Comparison of velocity streamlines in various carotid bifurcation models during early systole at different outlet pressures

3.2 Static Pressure

The pressure contours of the three models are shown in Figure 8. The distribution of pressure is not uniform in all three cases. During peak systole, Model-1 with LBP had minimum pressure at ECA and ICA outlets whereas maximum pressure was observed in the inner wall of bifurcation. Along the length of the straight portion of CCA circumferential pressure distribution was uniform whereas at curved locations it varied significantly along with ECA and ICA [27,44]. It was observed in Model-2

with HBP, that minimum pressure location remains at the outlet of ICA and ECA. Along the length of CCA and ECA pressure distribution was observed to be in a range with magnitude varying near mean pressure value. Model-3 with NBP also had minimum pressure at the outlet of ICA and ECA whereas maximum pressure at the inner wall of bifurcation and at the origin of ECA the pressure distribution is slightly large. Along the length of ECA, CCA, and ICA pressure distribution is not uniform [45]. While three pressure conditions were compared the location of max pressure remains to be the inner wall of bifurcation and minimum pressure at the outlets of ICA and ECA.

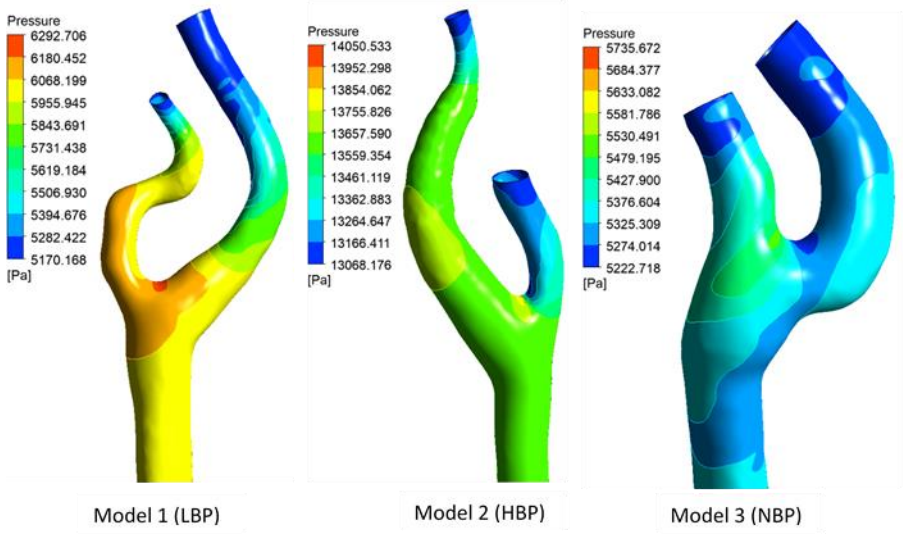

Fig. 8. Pressure contours comparison in carotid bifurcation models during peak systole at different outlet pressures

3.3 Helicity Patterns

Figure 9 shows the isosurface of helicity patterns demonstrating positive and negative flows in the carotid artery models. The intravascular flow structure profile within the carotid bifurcation system is particularly characterized by a helical pattern. The helical flow patterns are visualized by setting a threshold of ± 1. The negative values represent counterclockwise flow whereas the positive represent clockwise, the values near zero show lesser helical intensities [44,45]. The low-intensity helicity appears to start at the flow divider region and develops into the sinus region in the ICA. The observations are similar for all the BP cases qualitatively, however, the flow reversal increases with increased BP. The notable difference is that the negative flow volume is relatively larger in HBP compared to the LBP case in the ICA. In the carotid artery, a large number of intravascular flow structures are precisely defined by helical patterns. 4D complex helical flow is reduced to 3D and defined with numerical data as mentioned in works of literature [7,39,46]. Regions having lesser helical intensity seemingly start from the sinus and intensified in the lower ICA. Helical patterns of flow look disoriented and irregular in stenosed cases. Patterns of low helical intensity present in larger surface during early diastole.

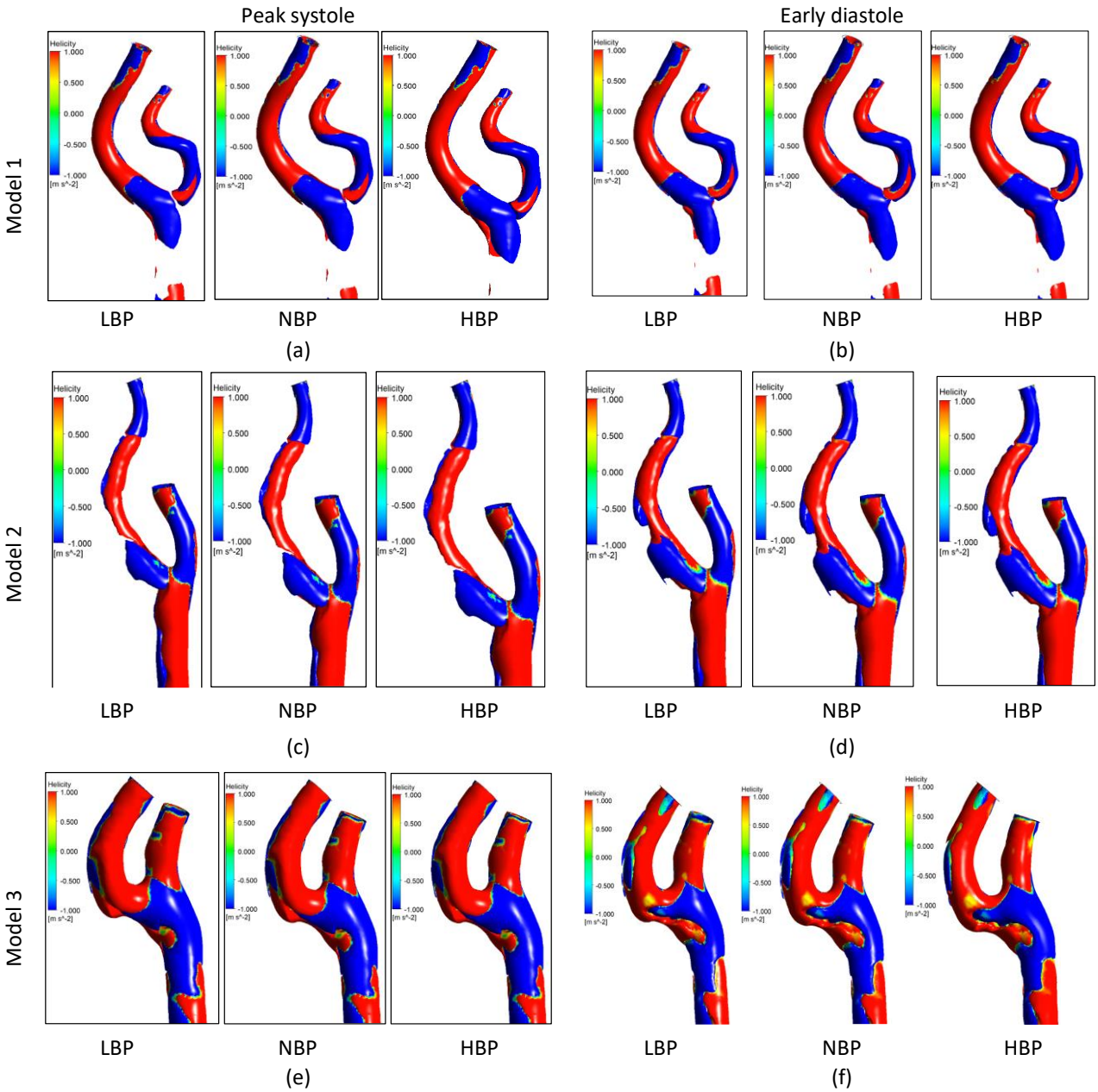

Fig. 9. Helicity plots for HBP, NBP, and LBP condition, (a) peak systole of model 1, (b) early diastole of model 1, (c) peak systole of model 2, (d) early diastole of model 2, (e) peak systole of model 3, (f) early diastole of model 3

3.4 Vorticity

Figure 10 shows vorticity contours in carotid artery models. The study of vorticity contours which is the absolute value of dot product of velocity and vorticity vector is of prime importance to understanding the flow patterns in the arterial tree. The development of three-dimensional secondary flow fields influences the flow near to the wall. The fluid flow along the axis perpendicular to the wall generates pressure gradients in its surrounding area [17,24,47]. The boundary layer upstream of CCA undergoes three-dimensional flow separation as seen in the figure above (helicity). The flow recirculates downstream of the separation line for a vortex zone. As the flow approaches the apex of the bifurcation zone, it deviates into reverse directions perpendicular to its actual path,

demonstrating vortex formation. Therefore, it was observed that the flow separation occurs at the lateral wall of the ICA at the apex at the corner where the ECA is branching.

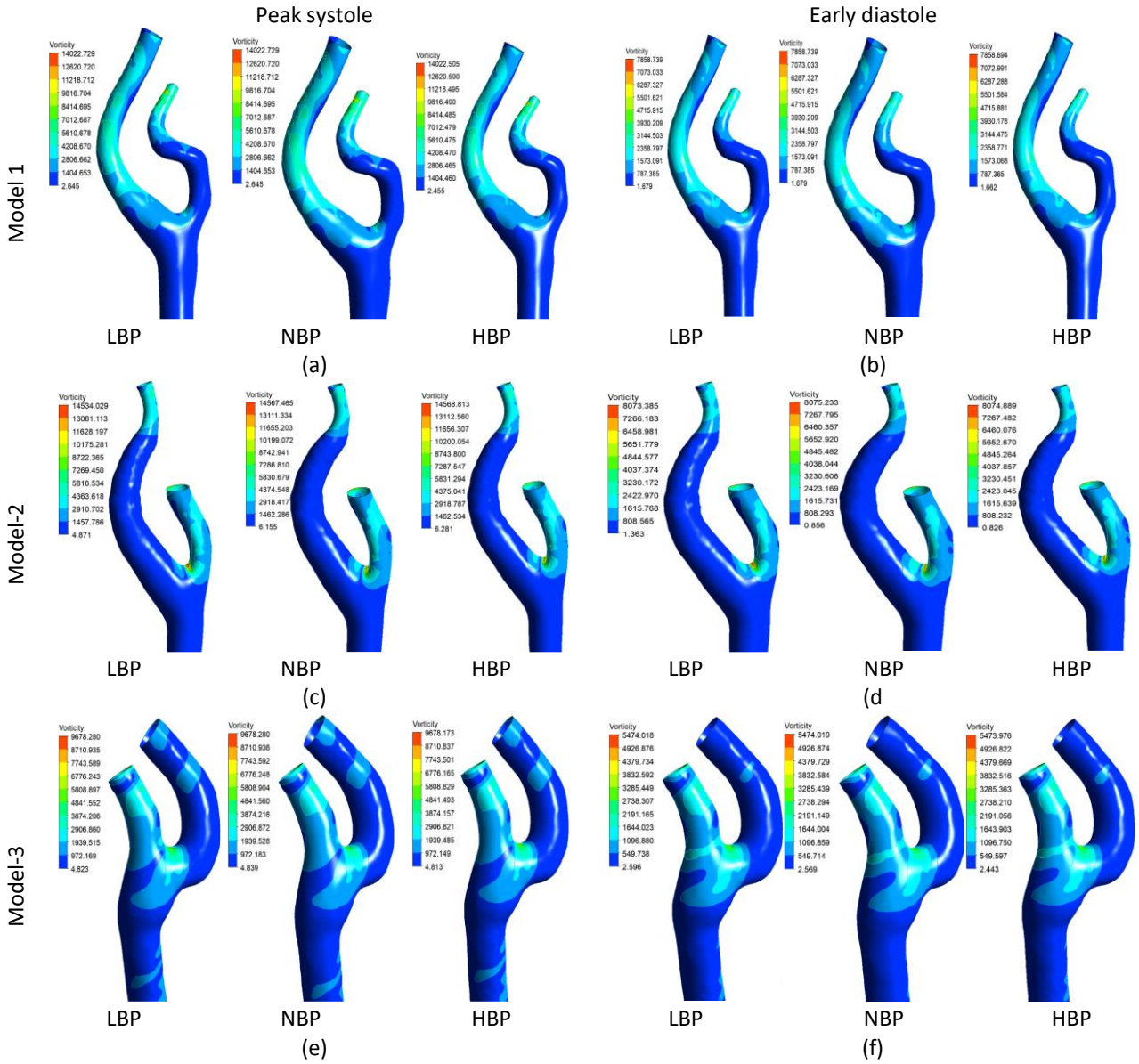

Fig. 10. Vorticity plot for HBP, NBP, and LBP condition, (a) peak systole of model 1, (b) early diastole of model 1, (c) peak systole of model 2, (d) early diastole of model 2, (e) peak systole of model 3, (f) early diastole of model 3

3.5 Time-averaged Wall Shear Stress

The TAWSS parameter is a function of wall shear stress is given below, where T is the period of the cardiac cycle [40].

$$TAWSS = \frac{1}{T}\int_0^T |WSS|\, dt \tag{3}$$

The TAWSS is a temporal average of the WSS over a full cardiac cycle. The variation of WSS throughout a cardiac cycle can be determined using TAWSS and described as shown in the Figure 11.

To obtain TAWSS, magnitude of WSS vector is integrated at each node using cardiac cycle as the interval [33,45,48].

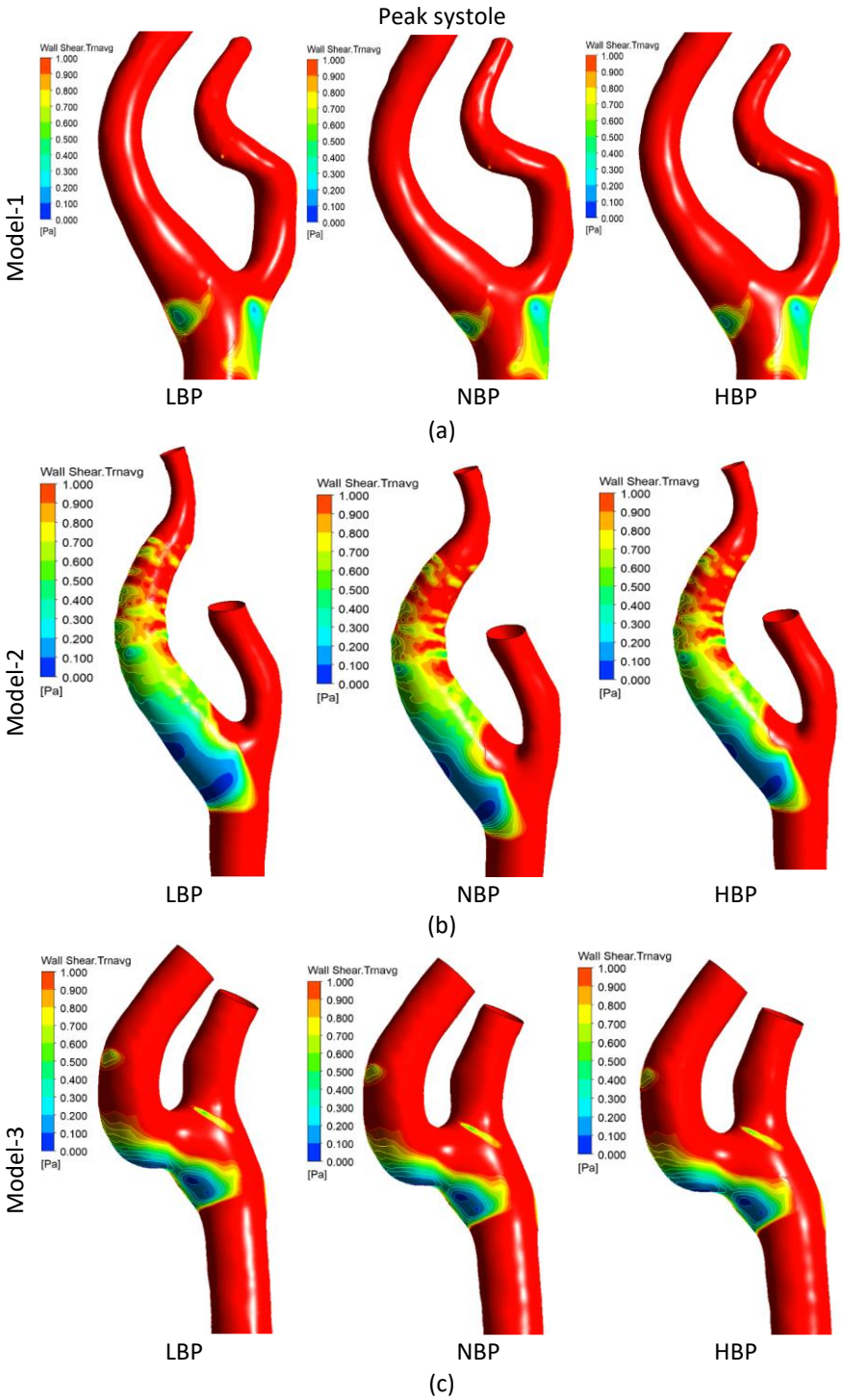

Fig. 11. Time average wall shear stress plot for HBP, NBP, and LBP condition in three carotid bifurcation models

Atherosclerosis is more likely to develop in areas with low TAWSS values [6,41]. In model 1 during early diastole for all 3 types of pressure conditions, the region or surface area having a low range of TAWSS is greater when compared with the plot taken at peak systole which implies that blood flow during early diastole has less value of TAWSS which may lead to the formation of atherosclerosis. In

models 2 and 3, peak systole has a larger surface area having less TAWSS compared to early diastole for all pressure conditions. TAWSS values for different pressure condition for every model is observed to be similar which implies that values of TAWSS is having less significance for change pressure condition. When a region having less TAWSS is observed, in model 1 surface area having less TAWSS is located near the bifurcation region towards ECA. In models 2 and 3 location of less TAWSS is towards ICA in bifurcation region, from this observation geometry of the carotid artery plays a major role in Haemodynamics of the artery. The TAWSS is a temporal average of the WSS over a full cardiac cycle. The variation of WSS throughout a cardiac cycle can be determined using TAWSS and described as shown in the Figure 11. To obtain TAWSS, the magnitude of the WSS vector is integrated at each node using the cardiac cycle as the interval. Atherosclerosis is more likely to develop in areas with low TAWSS values [41,48,49]. In model 1 during early diastole for all 3 types of pressure conditions, the region or surface area having a low range of TAWSS is greater when compared with a plot taken at peak systole which implies that blood flow during early diastole has less value of TAWSS which may lead to the formation of atherosclerosis. In models 2 and 3, peak systole has a larger surface area having less TAWSS as compared to early diastole for all pressure conditions. TAWSS values for different pressure condition for every model is observed to be similar which implies that values of TAWSS is having less significance for change pressure condition. When a region having less TAWSS is observed, in model 1 surface area having less TAWSS is located near the bifurcation region towards ECA. In models 2 and 3 location of less TAWSS is towards ICA in the bifurcation region, from this observation geometry of the carotid artery plays a major role in the Haemodynamics of the artery [50].

4. Conclusions

In the present study, three different geometric shapes of the carotid bifurcation system are numerically investigated under different blood pressures. Haemodynamic parameters such as velocity, pressure, helicity, vorticity, and time-averaged wall shear stress have been evaluated and discussed. Due to the different geometric profiles of ICA branching in all the three models, higher flow is observed in ICA in contrast to ECA flow distribution. The steep velocity gradient at the bifurcation region and reversed flow patterns along the outer wall of ICA are also exhibited in all three models. However, under different blood pressure conditions, maximum pressure remains along the inner wall of bifurcation, and the minimum pressure is observed at the distal side of ICA and ECA branching. Further, there is a qualitative behavior of helicity in the bifurcation region, and flow reversal increases with the higher blood pressure. It is also seen that negative flow volume is relatively larger in HBP compared to the LBP case in the ICA. Vortex formation has demonstrated significance in all the models when the flow approaches the apex of bifurcation and later diverges into reverse directions to the initial path. It is established that atherosclerosis is more likely to develop in areas with low TAWSS values especially spread to larger surface during peak systole. It is also observed that, values of TAWSS have less significance irrespective of altered pressured conditions especially at the bifurcation zone. Overall, it is demonstrated well that the geometry at carotid bifurcation zone plays major role in Haemodynamics of the artery. This study can be further explored by considering the influence of elastic artery and non-Newtonian blood flow assumptions and can be extended to the stenosed cases.

Acknowledgement

This work is supported by DST-International Bilateral Cooperation Division grant: DST/JSPS/P-293/2019. The authors would like to express their gratitude and sincere appreciation to DST-JSPS for supporting this study.

References

[1] World Health Organization. "Hearts: technical package for cardiovascular disease management in primary health care." (2016).
[2] Reddy, K. Srinath. "Cardiovascular diseases in the developing countries: dimensions, determinants, dynamics and directions for public health action." *Public health nutrition* 5, no. 1a (2002): 231-237. https://doi.org/10.1079/PHN2001298
[3] Dustan, Harriet P. "50th anniversary historical article. Hypertension." *Journal of the American College of Cardiology* 35, no. 5 Suppl B (2000): 10B-12B. https://doi.org/10.1016/S0735-1097(00)80042-X
[4] Swirski, Filip K., and Matthias Nahrendorf. "Leukocyte behavior in atherosclerosis, myocardial infarction, and heart failure." *Science* 339, no. 6116 (2013): 161-166. https://doi.org/10.1126/science.1230719
[5] Frostegård, Johan. "Immunity, atherosclerosis and cardiovascular disease." *BMC medicine* 11, no. 1 (2013): 1-13. https://doi.org/10.1186/1741-7015-11-117
[6] James, Paul A., Suzanne Oparil, Barry L. Carter, William C. Cushman, Cheryl Dennison-Himmelfarb, Joel Handler, Daniel T. Lackland et al. "2014 evidence-based guideline for the management of high blood pressure in adults." *Jama* 311, no. 5 (2014): 507-520. https://doi.org/10.1001/jama.2013.284427
[7] Steinman, David A. "Image-based computational fluid dynamics modeling in realistic arterial geometries." *Annals of biomedical engineering* 30, no. 4 (2002): 483-497. https://doi.org/10.1114/1.1467679
[8] White, C. J. "Carotid stenting vs. endarterectomy." *J Am Coll Cardiol* 64 (2014): 722-3. https://doi.org/10.1016/j.jacc.2014.04.069
[9] Subramaniam, Thineshwaran, and Mohammad Rasidi Rasani. "Pulsatile CFD Numerical Simulation to investigate the effect of various degree and position of stenosis on carotid artery hemodynamics." *Journal of Advanced Research in Applied Sciences and Engineering Technology* 26, no. 2 (2022): 29-40. https://doi.org/10.37934/araset.26.2.2940
[10] Ramdan, Salman Aslam, Mohammad Rasidi Rasani, Thinesh Subramaniam, Ahmad Sobri Muda, Ahmad Fazli Abdul Aziz, Tuan Mohammad Yusoff Shah Tuan Ya, Hazim Moria, Mohd Faizal Mat Tahir, and Mohd Zaki Nuawi. "Blood Flow Acoustics in Carotid Artery." *Journal of Advanced Research in Fluid Mechanics and Thermal Sciences* 94, no. 1 (2022): 28-44. https://doi.org/10.37934/arfmts.94.1.2844
[11] Strony, J., Beaudoin, A., Brands, D., and Adelman, B. "Analysis of shear stress and hemodynamic factors in a model of coronary artery stenosis and thrombosis." *American Journal of Physiology-Heart and Circulatory Physiology* 265, no. 5 (1993): H1787-H1796. https://doi.org/10.1152/ajpheart.1993.265.5.H1787
[12] Perktold, Karl, and Gerhard Rappitsch. "Computer simulation of local blood flow and vessel mechanics in a compliant carotid artery bifurcation model." *Journal of biomechanics* 28, no. 7 (1995): 845-856. https://doi.org/10.1016/0021-9290(95)95273-8
[13] Hegde, Pranav, A. B. V. Barboza, SM Abdul Khader, Raghuvir Pai, Masaaki Tamagawa, Ravindra Prabhu, and D. Srikanth Rao. "Numerical Analysis on A Non-Critical Stenosis in Renal Artery." *Journal of Advanced Research in Fluid Mechanics and Thermal Sciences* 88, no. 3 (2021): 31-48. https://doi.org/10.37934/arfmts.88.3.3148
[14] Bathe, R. K. M. (1999). Computer simulation of local blood flow and vessel mechanics in a compliant carotid artery bifurcation model. Journal of Biomechanics, J. Biomech. Eng. Trans. ASME, vol. 121, pp. 361-369.
[15] Al-Azawy, Mohammed Ghalib, Saleem Khalefa Kadhim, and Azzam Sabah Hameed. "Newtonian and non-newtonian blood rheology inside a model of stenosis." *CFD Letters* 12, no. 11 (2020): 27-36. https://doi.org/10.37934/cfdl.12.11.2736
[16] Zain, Norliza Mohd, Zuhaila Ismail, and Peter Johnston. "A Stabilized Finite Element Formulation of Non-Newtonian Fluid Model of Blood Flow in A Bifurcated Channel with Overlapping Stenosis." *Journal of Advanced Research in Fluid Mechanics and Thermal Sciences* 88, no. 1 (2021): 126-139. https://doi.org/10.37934/arfmts.88.1.126139
[17] Tang, Dalin, Chun Yang, Shunichi Kobayashi, Jie Zheng, and Raymond P. Vito. "Effect of stenosis asymmetry on blood flow and artery compression: a three-dimensional fluid-structure interaction model." *Annals of biomedical engineering* 31, no. 10 (2003): 1182-1193. https://doi.org/10.1114/1.1615577
[18] Torii, Ryo, Marie Oshima, Toshio Kobayashi, Kiyoshi Takagi, and Tayfun E. Tezduyar. "Fluid–structure interaction modeling of aneurysmal conditions with high and normal blood pressures." *Computational Mechanics* 38, no. 4 (2006): 482-490.. https://doi.org/10.1007/s00466-006-0065-6

[19] Fu, Yulin, Aike Qiao, and Long Jin. "The influence of hemodynamics on the ulceration plaques of carotid artery stenosis." *Journal of Mechanics in Medicine and Biology* 15, no. 01 (2015): 1550008. https://doi.org/10.1142/S0219519415500086

[20] Li, Cong-Hui, Bu-Lang Gao, Ji-Wei Wang, Jian-Feng Liu, Hui Li, and Song-Tao Yang. "Hemodynamic factors affecting carotid sinus atherosclerotic stenosis." *World Neurosurgery* 121 (2019): e262-e276. https://doi.org/10.1016/j.wneu.2018.09.091

[21] Gallo, Diego, David A. Steinman, Payam B. Bijari, and Umberto Morbiducci. "Helical flow in carotid bifurcation as surrogate marker of exposure to disturbed shear." *Journal of biomechanics* 45, no. 14 (2012): 2398-2404. https://doi.org/10.1016/j.jbiomech.2012.07.007

[22] Lim, Sheh Hong, Mohd Azrul Hisham Mohd Adib, Mohd Shafie Abdullah, Nur Hartini Mohd Taib, Radhiana Hassan, and Azian Abd Aziz. "Study of extracted geometry effect on patient-specific cerebral aneurysm model with different threshold coefficient (Cthres)." *CFD Letters* 12, no. 10 (2020): 1-14. https://doi.org/10.37934/cfdl.12.10.114

[23] Seman, Che Mohammad Hafizal Muzammil Che, Nur Ayuni Marzuki, Nofrizalidris Darlis, Noraini Marsi, Zuliazura Mohd Salleh, Izuan Amin Ishak, Ishkrizat Taib, and Safra Liyana Sukiman. "Comparison of Hemodynamic Performances Between Commercial Available Stents Design on Stenosed Femoropopliteal Artery." *CFD Letters* 12, no. 7 (2020): 17-25. https://doi.org/10.37934/cfdl.12.7.1725

[24] Gallo, Diego, David A. Steinman, and Umberto Morbiducci. "Insights into the co-localization of magnitude-based versus direction-based indicators of disturbed shear at the carotid bifurcation." *Journal of biomechanics* 49, no. 12 (2016): 2413-2419. https://doi.org/10.1016/j.jbiomech.2016.02.010

[25] Jamali, Muhammad Sabaruddin Ahmad, Zuhaila Ismail, and Norsarahaida Saidina Amin. "Effect of Different Types of Stenosis on Generalized Power Law Model of Blood Flow in a Bifurcated Artery." *Journal of Advanced Research in Fluid Mechanics and Thermal Sciences* 87, no. 3 (2021): 172-183. https://doi.org/10.37934/arfmts.87.3.172183

[26] Moyle, Keri R., Luca Antiga, and David A. Steinman. "Inlet conditions for image-based CFD models of the carotid bifurcation: is it reasonable to assume fully developed flow?." *Journal of biomechanical engineering* 128, no. 3 (2006): 371-379. https://doi.org/10.1115/1.2187035

[27] Urevc, Janez, Iztok Žun, Milan Brumen, and Boris Štok. "Modeling the effect of red blood cells deformability on blood flow conditions in human carotid artery bifurcation." *Journal of Biomechanical Engineering* 139, no. 1 (2017): 011011. https://doi.org/10.1115/1.4035122

[28] Campbell, Ian C., Jared Ries, Saurabh S. Dhawan, Arshed A. Quyyumi, W. Robert Taylor, and John N. Oshinski. "Effect of inlet velocity profiles on patient-specific computational fluid dynamics simulations of the carotid bifurcation." *Journal of biomechanical engineering* 134, no. 5 (2012). https://doi.org/10.1115/1.4006681

[29] Morbiducci, Umberto, Diego Gallo, Diana Massai, Filippo Consolo, Raffaele Ponzini, Luca Antiga, Cristina Bignardi, Marco A. Deriu, and Alberto Redaelli. "Outflow conditions for image-based hemodynamic models of the carotid bifurcation: implications for indicators of abnormal flow." *Journal of biomechanical engineering* 132, no. 9 (2010). https://doi.org/10.1115/1.4001886

[30] Bevan, Rhodri, P. Nithiarasu, Igor Sazonov, Raoul van Loon, Heyman Luckraz, Michael Collins, and Andrew Garnham. "Influences of domain extensions to a moderately stenosed patient-specific carotid bifurcation: Investigation of wall quantities." *International Journal of Numerical Methods for Heat & Fluid Flow* (2011). https://doi.org/10.1108/09615531111177741

[31] Razhali, Nur Farahalya, and Ishkrizat Taib. "Analysis of Hemodynamic on Different Stent Strut Configurations in Femoral Popliteal Artery." *CFD Letters* 14, no. 3 (2022): 119-128. https://doi.org/10.37934/cfdl.14.3.119128

[32] Gharahi, Hamidreza, Byron A. Zambrano, David C. Zhu, J. Kevin DeMarco, and Seungik Baek. "Computational fluid dynamic simulation of human carotid artery bifurcation based on anatomy and volumetric blood flow rate measured with magnetic resonance imaging." *International journal of advances in engineering sciences and applied mathematics* 8, no. 1 (2016): 46-60. https://doi.org/10.1007/s12572-016-0161-6

[33] Hegde, Pranav, SM Abdul Khader, Raghuvir Pai, Masaaki Tamagawa, Ravindra Prabhu, Nitesh Kumar, and Kamarul Arifin Ahmad. "CFD Analysis on Effect of Angulation in A Healthy Abdominal Aorta-Renal Artery Junction." *Journal of Advanced Research in Fluid Mechanics and Thermal Sciences* 88, no. 1 (2021): 149-165. https://doi.org/10.37934/arfmts.88.1.149165

[34] Sousa, Luísa C., Catarina F. Castro, Carlos C. António, Fernando Sousa, Rosa Santos, Pedro Castro, and Elsa Azevedo. "Computational simulation of carotid stenosis and flow dynamics based on patient ultrasound data–A new tool for risk assessment and surgical planning." *Advances in medical sciences* 61, no. 1 (2016): 32-39. https://doi.org/10.1016/j.advms.2015.07.009

[35] Algabri, Yousif A., Surapong Chatpun, and Ishkrizat Taib. "An investigation of pulsatile blood flow in an angulated neck of abdominal aortic aneurysm using computational fluid dynamics." *Journal of Advanced Research in Fluid Mechanics and Thermal Sciences* 57, no. 2 (2019): 265-274.

[36] Paisal, Muhammad Sufyan Amir, Ishkrizat Taib, Ahmad Mubarak Tajul Arifin, and Nofrizalidris Darlis. "An analysis of blood pressure waveform using windkessel model for normotensive and hypertensive conditions in carotid artery." *Journal of Advanced Research in Fluid Mechanics and Thermal Sciences* 57, no. 1 (2019): 69-85.
[37] Bit, Arindam, Dushali Ghagare, Albert A. Rizvanov, and Himadri Chattopadhyay. "Assessment of influences of stenoses in right carotid artery on left carotid artery using wall stress marker." *BioMed Research International* 2017 (2017). https://doi.org/10.1155/2017/2935195
[38] Bruno, G., and C. Vergara. "Computational comparison between Newtonian and non-Newtonian blood rheologies in stenotic vessels''. Biomedical Technology." (2018): 169-183. https://doi.org/10.1007/978-3-319-59548-1_10
[39] Lee, Seung E., Sang-Wook Lee, Paul F. Fischer, Hisham S. Bassiouny, and Francis Loth. "Direct numerical simulation of transitional flow in a stenosed carotid bifurcation." *Journal of biomechanics* 41, no. 11 (2008): 2551-2561. https://doi.org/10.1016/j.jbiomech.2008.03.038
[40] Rayz, Vitaliy L., Stanley A. Berger, and David Saloner. "Transitional flows in arterial fluid dynamics." *Computer methods in applied mechanics and engineering* 196, no. 31-32 (2007): 3043-3048. https://doi.org/10.1016/j.cma.2006.10.014
[41] Harrison, Gareth J., Thien V. How, Robert J. Poole, John A. Brennan, Jagjeeth B. Naik, S. Rao Vallabhaneni, and Robert K. Fisher. "Closure technique after carotid endarterectomy influences local hemodynamics." *Journal of Vascular Surgery* 60, no. 2 (2014): 418-427. https://doi.org/10.1016/j.jvs.2014.01.069
[42] Guerciotti, Bruno, Christian Vergara, Laura Azzimonti, Laura Forzenigo, Adelaide Buora, Piero Biondetti, and Maurizio Domanin. "Computational study of the fluid-dynamics in carotids before and after endarterectomy." *Journal of biomechanics* 49, no. 1 (2016): 26-38. https://doi.org/10.1016/j.jbiomech.2015.11.009
[43] Domanin, M., D. Bissacco, D. Le Van, and Christian Vergara. "Computational fluid-dynamic comparison between patch-based and direct suture closure techniques after carotid endarterectomy." (2018): 887-897. https://doi.org/10.1016/j.jvs.2017.08.094
[44] Sia, Sheau Fung, Xuemei Zhao, Yong Yu, and Yu Zhang. "Multiphase particle-in-cell simulation in severe internal carotid artery stenosis." *Powder Technology* 358 (2019): 62-67. https://doi.org/10.1016/j.powtec.2018.07.091
[45] Kumar, Nitesh, Abdul Khader, Raghuvir Pai, Panayiotis Kyriacou, Sanowar Khan, and Prakashini Koteshwara. "Computational fluid dynamic study on effect of Carreau-Yasuda and Newtonian blood viscosity models on hemodynamic parameters." *Journal of Computational Methods in Sciences and Engineering* 19, no. 2 (2019): 465-477. https://doi.org/10.3233/JCM-181004
[46] Tang, Dalin, Chun Yang, Yan Huang, and David N. Ku. "Wall stress and strain analysis using a three-dimensional thick-wall model with fluid–structure interactions for blood flow in carotid arteries with stenoses." *Computers & structures* 72, no. 1-3 (1999): 341-356. https://doi.org/10.1016/S0045-7949(99)00009-7
[47] Li, Z., and C. Kleinstreuer. "Fluid-structure interaction effects on sac-blood pressure and wall stress in a stented aneurysm." (2005): 662-671. https://doi.org/10.1115/1.1934040
[48] Garcia, Julio, Alex J. Barker, Jeremy D. Collins, James C. Carr, and Michael Markl. "Volumetric quantification of absolute local normalized helicity in patients with bicuspid aortic valve and aortic dilatation." *Magnetic resonance in medicine* 78, no. 2 (2017): 689-701. https://doi.org/10.1016/j.physbeh.2017.03.040
[49] Massai, Diana, Giulia Soloperto, Diego Gallo, Xiao Yun Xu, and Umberto Morbiducci. "Shear-induced platelet activation and its relationship with blood flow topology in a numerical model of stenosed carotid bifurcation." *European Journal of Mechanics-B/Fluids* 35 (2012): 92-101. https://doi.org/10.1016/j.euromechflu.2012.03.011
[50] Moradicheghamahi, Jafar, Jaber Sadeghiseraji, and Mehdi Jahangiri. "Numerical solution of the Pulsatile, non-Newtonian and turbulent blood flow in a patient specific elastic carotid artery." *International Journal of Mechanical Sciences* 150 (2019): 393-403. https://doi.org/10.1016/j.ijmecsci.2018.10.046